Design and Hardware-In-the-Loop Validation of a Fault-Tolerant Y* Flight Control Law*

Sérgio Waitman[1], Andrés Marcos[1] and Masayuki Sato[2]

***Abstract*— This article presents the design and validation of a fault-tolerant Y* flight controller for the Japanese Aerospace Exploration Agency's (JAXA) Multi-Purpose Aviation Laboratory-α (MuPAL-α) aircraft. A structured H_∞ controller is synthesized by using non-smooth optimization to address performance and robustness constraints (specifically, uncertain actuator delays and varying airspeed) as well as loss-of-efficiency faults of a specific range with reduced online numerical complexity. The performance of the closed-loop system is validated through hardware-in-the-loop (HIL) simulations using the actual MuPAL-α aircraft, and they show that an improved fault tolerant capability is achieved when compared to Y* design robust only against the actuator delays.**

I. INTRODUCTION

This paper presents the design and hardware-in-the-loop (HIL) testing of a fault-tolerant Y* controller for the Japanese Aerospace Exploration Agency's (JAXA) Multi-Purpose Aviation Laboratory-α (MuPAL-α) aircraft [1], designed using the robust structured H_∞ approach [2]. The Y* control laws are the most extensively used in commercial aircraft for the control of the lateral/directional motion [3]. They are based on classical control architectures and were developed based on the understanding of the manner in which pilots physically fly [4]. Recently, with the advent of the structured H_∞ synthesis approach [5], [6], new research on the design of these laws has been undertaken by both academia [7], [8] and industry [9], [10]. This article continues that work and serves to increase the technological readiness level (TRL) of the synthesis approach. The presented design is synthesized with the aim of providing robustness against airspeed and uncertain actuator delay (which models the presence of uncertain nonlinearities such as backlash and dead time [1]), and is validated in the MuPAL-α aircraft's HIL test environment. The fault cases considered in the design phase are loss of efficiency (LoE) on the aileron and rudder actuators ranging from nominal (0% LoE) up to 80% LoE, on each control surface individually and simultaneously. Two controllers are designed, both composed of feedback and feedforward gains: K-ROB and K-FTC. The former is a robust controller against airspeed and uncertain actuator delay, while the latter is a fault-tolerant controller that, in addition to the design specifications for K-ROB, explicitly takes into account the actuator efficiency faults. This work is part of the European H2020 and Japan NEDO collaborative project VISION ("Validation of Integrated Safety-enhanced Intelligent flight cONtrol") which aims to study and validate fault-tolerant approaches for aircraft.

The layout of the article is as follows: In Section II the lateral/directional models of the aircraft are presented. This is followed in Section III with the presentation of the design of the robust and fault-tolerant controllers. Section IV presents the verification with linear simulations and Section V concludes with the validation in HIL simulations.

II. AIRCRAFT MODEL

The lateral/directional dynamics of the aircraft are described by linear time-invariant models obtained from trimming and linearization in cruise level flight at 5000 ft. Trimming was performed at speeds ranging from 100 to 200 knots. The lateral/directional models have 4 states (inertial sway speed v_i (m/s), roll rate p (rad/s), roll angle ϕ (rad) and yaw rate r (rad/s)), two inputs (aileron, δ_a, and rudder, δ_r, deflections (rad)) and as outputs the vector $[\ v_a \quad p \quad \phi \quad r\ ]^T$, where v_a is the sway airspeed. A pole-zero map of the lateral dynamics with respect to varying speed is shown in Fig. 1, with a zoom on the spiral mode. It can be seen that this mode is unstable in lower speeds. For the Y* design model, the sway airspeed output is substituted by the sideslip angle, β (rad), by using the approximation (valid for small β) $\beta = v_a/V_{\text{EAS}}$, where V_{EAS} is the equivalent airspeed at each corresponding trim point. The actuator dynamics are modelled as first-order systems with delay:

$$\begin{aligned}\delta_a &= e^{-T_{d,a}s}\frac{0.67}{0.04s+1}\delta_{a,c}\\ \delta_r &= e^{-T_{d,r}s}\frac{0.83}{0.07s+1}\delta_{r,c}\end{aligned} \tag{1}$$

These actuator models differ from the ones considered in [1]. This is due to the fact that the controllers are validated in HIL, and hence the effect of the dynamic pressure is not considered. The delay is treated as an uncertain parameter for synthesis purposes, and is taken to belong to:

$$\begin{aligned}T_{d,a} &\in [0.06, 0.40]\ \text{s}\\ T_{d,r} &\in [0.06, 0.20]\ \text{s}.\end{aligned} \tag{2}$$

III. CONTROLLER DESIGN

The control structure adopted for the lateral dynamics is similar to the Y* law in [3]. In this control strategy, the pilot

*This work has received funding from the EU Horizon 2020 research and innovation programme (GA N. 690811) and the Japan New Energy and Development Organization (GA N. 062800), as a part of the EU/Japan research project VISION.

[1]Sérgio Waitman and Andrés Marcos are with the Aerospace Engineering Department, University of Bristol, BS8 1TR Bristol, UK {sergio.waitman,andres.marcos}@bristol.ac.uk

[2]Masayuki Sato is with the Aeronautical Technology Directorate, Japan Aerospace Exploration Agency, Mitaka, Tokyo 181-0015, Japan. sato.masayuki@jaxa.jp

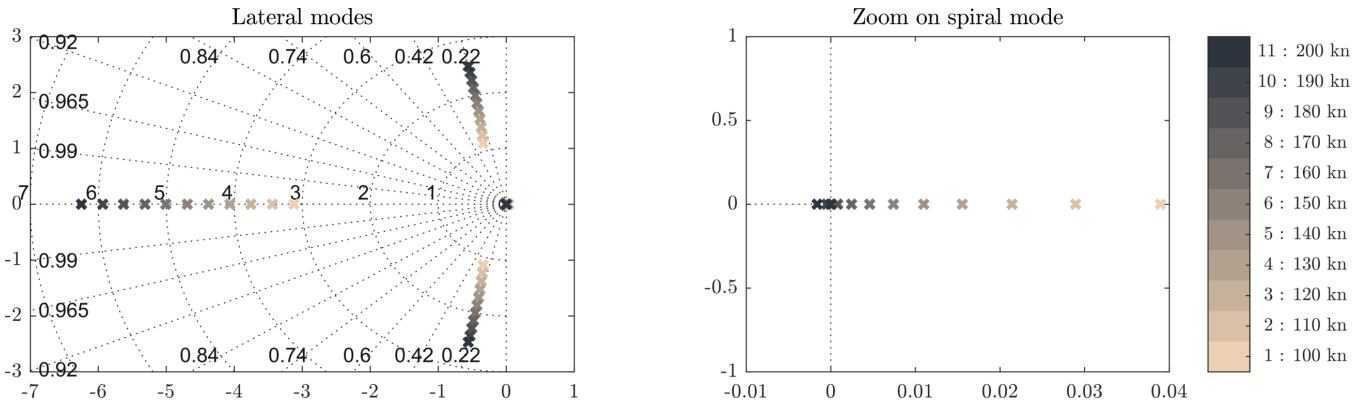

Fig. 1: Pole-zero map of lateral/directional dynamics with varying speed.

provides roll rate commands p_c via lateral displacements of the stick. The roll rate command is then transformed into a roll angle reference ϕ_c, where a direct gain k is added to improve the maneuverability of the aircraft. The pedal commands a combination of sideslip (β_c) and roll angle commands to retain some of the natural response of the aircraft, thus facilitating the instinctive response of the pilot. The controller consists of a static feedback term and a static feedforward gain, as well as a dynamic block translating the pilot's commands into ϕ_c and β_c, see Fig. 2. The controller designed for the MuPAL-α is augmented with two integrators on the tracking error of the roll and sideslip angles, respectively e_ϕ and e_β. This is done to ensure appropriate tracking of constant bank angles and zero sideslip for coordinated turns.

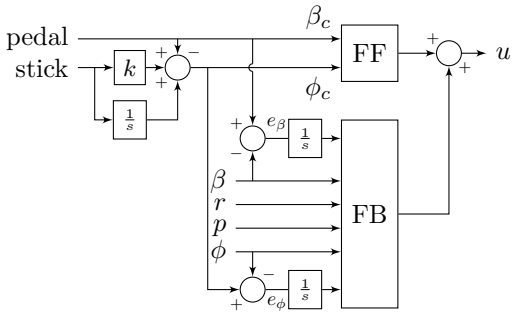

Fig. 2: Y* design controller structure.

The control design objectives are:

O1 Roll angle tracking
- Settling time: 8 s.
- Steady-state error: 0°.

O2 Sideslip angle tracking
- Settling time: 5 s.
- Steady-state error: 0°.

O3 Decoupling
- β response to ϕ_c step between $\pm 0.05°$.
- ϕ response to β_c step between $\pm 0.5°$.

O4 Robustness
- Time delay as in (2).
- $V_{\text{EAS}} \in [100, 160]$ knots.

The designs use the set of LTI plants (100, 110, ..., 150, and 160 knots). The faulty actuators are modelled as the first-order transfer functions in (1), but augmented with gains $k_{\text{eff},a}$ and $k_{\text{eff},r}$, respectively for aileron and rudder, which range from 1 (nominal) to 0.2 (80% LoE). These gains can be used to consider a particular fault case in the design, and are also used for simulating the faults in the linear and HIL simulations.

A. Robust controller (K-ROB)

1) Feedback and feedforward gains: In order to design the controller, the above specifications must be translated into weighting functions to constrain the H_∞ optimization problem. The adopted generalized plant structure for controller design is shown in Fig. 3. The signals considered are the reference $r = (\phi_c, \beta_c)$, control effort $u = (\delta_a, \delta_r)$, performance outputs $z = (\phi, \beta)$ and tracking errors $e = (e_\phi, e_\beta)$.

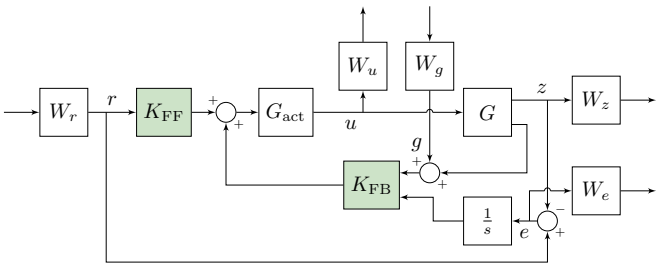

Fig. 3: Robust Y* design: Design interconnection.

A common controller for all models is synthesized using a multi-model approach [11] (i.e. using the models at $V_{\text{EAS}} =$ 120 and 160 knots) and a second-order Padé approximation of the maximum time-delay of each actuator. This airspeed multi-model and time-delay approximation set-up addresses specification **O4**.

The tracking objectives **O1** and **O2** are enforced via $W_e = \text{diag}(W_{e1}, W_{e2})$, with $W_{e1} = (0.6s+1.325)/(s+0.013)$ and $W_{e2} = (0.7s+1.183)/(s+0.012)$, selected to ensure that the response time is adequate. The control effort is tuned with W_u, which for the aileron is $(2e3s+2.519e4)/(s+1.008e4)$ and for the rudder the same weight scaled by 10 (based on

expected deflection with respect to aileron and fine tuning). The constraint on the zero steady-state error is enforced by the addition of the two integrators. The reference weight $W_r = \mathrm{diag}(0.067, 0.5)$ is selected, based on the expected variations of 15° and 2° on ϕ and β, respectively, while W_z is fixed as the identity matrix. The decoupling constraint **O3** is added as a multi-plant constraint with the help of weights $W_{\phi_c \to \beta} = 50$ and $W_{\beta_c \to \phi} = 2$ acting on the closed-loop SISO transfer functions from ϕ_c to β and from β_c to ϕ (disregarding all other inputs and outputs), see Fig. 4. Finally, the gust weight $W_g = 5$ is added to constrain the transfer function from the gust input to the sideslip angle channel.

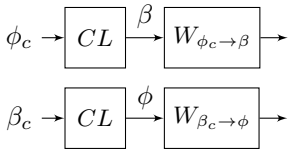

Fig. 4: Y* design: decoupling constraints.

The synthesis model has 14 states, 4 from the lateral dynamics, 4 from the actuator models, 2 from the added integrators, 2 from W_e and 2 from W_u. The controller is designed with the Matlab routine `hinfstruct` and achieves an H_∞ gain of 1.12. It shows good performance and robustness, as it will be seen in Section IV.

2) Stick/pedal allocation: Subsequently, the gain k between the roll rate command p_c and the translated roll angle command ϕ_c can be chosen. Based on simulations, the gain was fixed as $k = 1.3$ to ensure a compromise between the roll angle settling time and the corresponding overshoot.

B. Fault-tolerant controller (K-FTC)

The design of the fault-tolerant controller does not consider the gain k, which is maintained from the previous section. The actuator delay is once again taken into account by using a second-order Padé approximation of the maximum delay. The generalized plant for H_∞ design is simplified in comparison with the one used in Section III-A. This is done with the goal of simplifying the tuning of the controller, especially in the fine-tuning phase in between HIL tests. The new structure is presented in Fig. 5, and is comprised of two weights: W_r and W_e, on the reference input and tracking errors, respectively. With this structure, the sensitivity function is constrained to provide suitable tracking performance.

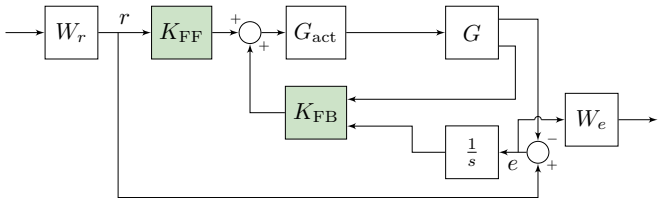

Fig. 5: FTC Y* design: Design interconnection.

The effect of gust is considered, but, unlike the approach in Section III-A, it is now considered as an additive disturbance to the sway speed. This is done to increase the fidelity of the model in representing the gust effect, in order to improve the gust suppression performance. In this new setting, the gust suppression specification is handled via the addition of an independent constraint pertaining specifically to the transfer function from the gust input to the roll and sideslip angles and to the roll and yaw rates ($[\phi \ \beta \ p \ r]$), with a constant input weight W_g (similar to the approach used to ensure the decoupling specification in the previous section), see Fig. 6. Finally, a last constraint is added on the location of the closed-loop poles, to impose a minimum damping. The controller K-FTC is designed to perform well under moderate aileron/rudder efficiency faults. To achieve this, a multi-model design is once again used, which considers the following conditions:

- Airspeed: 110 and 140 knots;
- Aileron LoE: 0% (nominal) and 40%.
- Rudder LoE: 0% (nominal) and 40%.

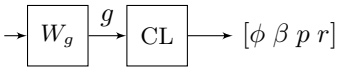

Fig. 6: FTC Y* design: gust suppression constraint.

In this way 8 plants, given by the combination of the above parameters, are used in the multi-model design. Different constraints are imposed on the nominal and faulty cases, to account for the fact that a reduced performance is expected in a fault scenario. First are presented the weights for the nominal case, which serve as a base for those in the faulty cases. The input weight is selected as $W_r = \mathrm{diag}(0.2, 1)$, to account for the heuristic that the pilot is around 5 to 10 times more sensitive for roll angle than sideslip angle variations (according to the last author's experience in flight tests with MuPAL-α without severe requirements for pilots). The tracking error weight is given by $W_e = \mathrm{diag}(W_{e1}, W_{e2})$, with $W_{e1} = (0.067s + 2.164)/(s + 0.065)$ and $W_{e2} = (0.350s + 0.592)/(s + 0.024)$, which are selected to impose an adequate tracking response. The weight $W_{\phi_c \to \beta} = 25$ is used to impose the decoupling from roll to sideslip, and the weight $W_{\beta_c \to \phi}$ was not used due to the decoupling from sideslip to roll being already satisfied. The weight on the gust performance is given by $W_g = 40$, selected after tuning and based on frequency response from the gust input to $[\phi \ \beta \ p \ r]$. Finally, a minimum damping of 0.71 is imposed on the closed-loop poles. These weights are used in the two nominal models (at 110 and 140 knots). In the 4 cases where only one of the actuators is faulty with 40% LoE (2 airspeeds times 2 actuator faults), the weights W_e, $W_{\phi_c \to \beta}$ and W_g are multiplied by a factor of 2/3, as is the minimum damping requirement. Finally, in the 2 cases (at 110 and 140 knots) where both actuators are faulty, the weights and minimum damping are multiplied by a factor of 1/2. As discussed above, this is done to relax the performance requirements in faulty scenarios, thus trading performance for fault tolerance. The structured H_∞ design problem is solved using the `systune` routine in

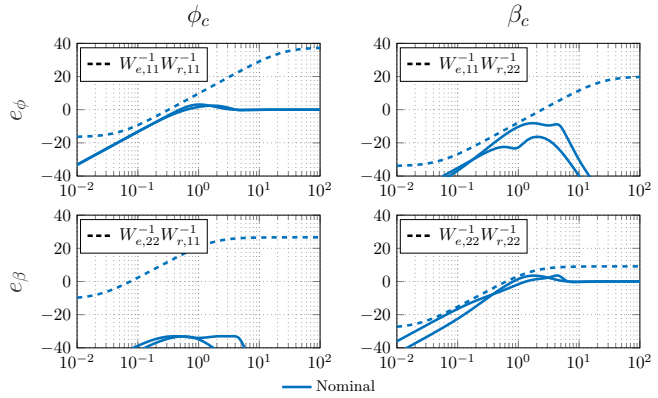

Fig. 7: Sensitivity function with K-ROB.

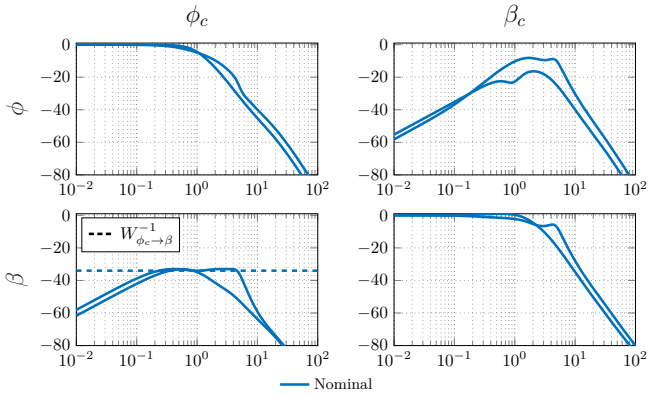

Fig. 8: Complementary Sensitivity function with K-ROB.

Matlab, using 5 random initial conditions for the feedback and feedforward gains. The optimization procedure yields an upper bound on the H_∞ gain of $\gamma = 1.42$, which indicates that some of the requirements were not met. Nonetheless, as it shall be illustrated in the next two sections, the controller provides adequate performance.

IV. VERIFICATION

This section presents the analysis of the robust (K-ROB) and fault-tolerant (K-FTC) controllers designed above. The analysis is done without the stick/pedal allocation block, thus focusing on the response to roll angle and sideslip commands. This is done to focus on the performance of the roll-angle tracking.

A. Frequency-domain responses

The frequency responses of the closed-loop system (with maximum actuator delay) between the reference input r and the outputs e and z are analyzed first. Figs. 7 and 8 show the sensitivity and complementary sensitivity functions with controller K-ROB, respectively. The full lines represent the frequency response of the closed-loop system, while the dashed lines represent the design weights. The first figure shows that the tracking specifications are satisfied. Figure 8 shows that the decoupling constraint is slightly violated from ϕ_c to β with respect to the defined weight (but the time simulations will show that it is still within acceptable bounds).

Now, the frequency response with the controller K-FTC in the nominal and design conditions are presented. Figs. 9 and 10 present the sensitivity and complementary sensitivity functions, respectively. The full lines represent the frequency response of the closed-loop system, and the dashed lines the corresponding weight used for each condition in the design. Fig. 9 shows that, overall, the tracking performance is satisfied, even in the presence of faults. Fig. 10 indicates that the decoupling constraint is not strictly met, but as it will be seen in the time response, the performance is adequate.

B. Time-domain responses

The time-domain responses of the closed-loop system are analyzed next. The performance is assessed via independent step responses to roll angle commands and roll angle/sideslip, both in nominal and faulty cases, in order to evaluate the fault-tolerance capabilities of both controllers. The response of the closed-loop system with K-ROB to a roll angle step command in nominal conditions is shown in Fig. 11, for different values of the uncertain delay (the step response to β_c is omitted due to limited space) . Only the speeds of 120 and 130 knots are shown for ease of visualization. The controller shows good tracking and decoupling performance according to the design specifications in the nominal case.

The same response, but now with K-FTC, both in nominal and 40% aileron LoE cases is shown in Figs. 12 and 13, again for different values of the uncertain delay. The results show that the roll angle response is similar in both cases, which indicates that the controller is indeed capable of maintaining maneuverability in fault scenarios. The decoupling with the sideslip angle is deteriorated in the LoE case, but still within the bounds set during design (red dashed lines).

Fig. 14 shows the response of the controlled aircraft with the K-FTC to doublet inputs on the roll angle and sideslip references, again using 4 different values of the uncertain delays and at the airspeeds of 120 and 130 knots. In this test, the LoE of aileron and rudder actuators are simulated as a ramp, starting from 0% at t = 0 and ending at 80% at

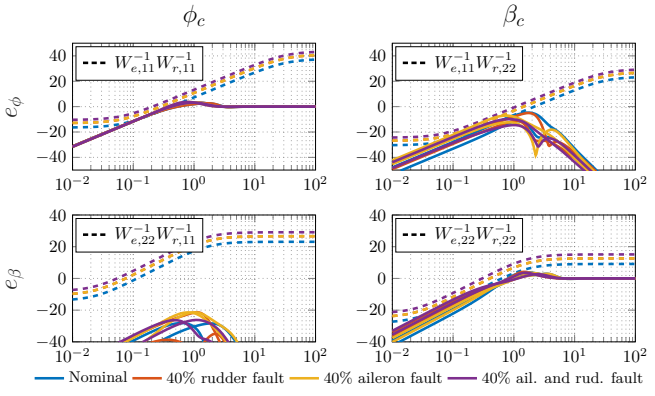

Fig. 9: Sensitivity function with K-FTC.

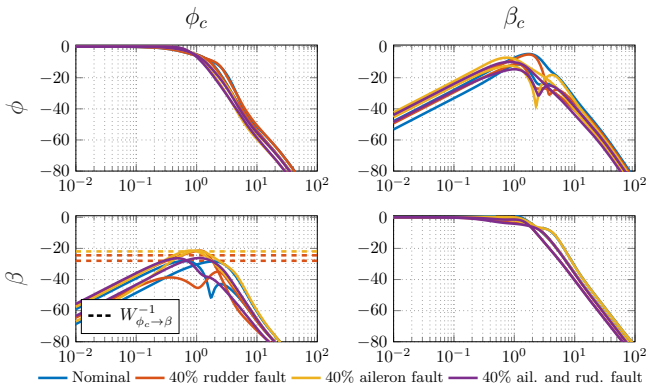

Fig. 10: Complementary sensitivity function with K-FTC.

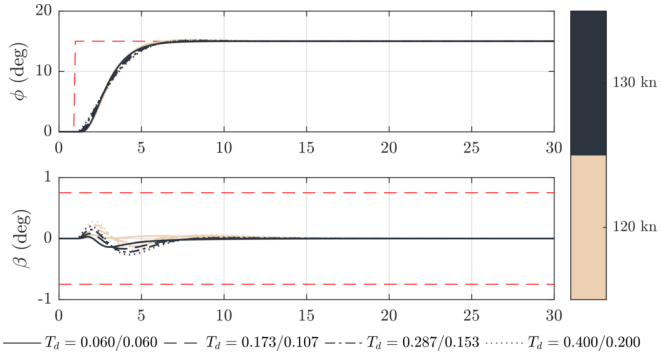

Fig. 11: Roll angle step response in no-fault conditions with K-ROB.

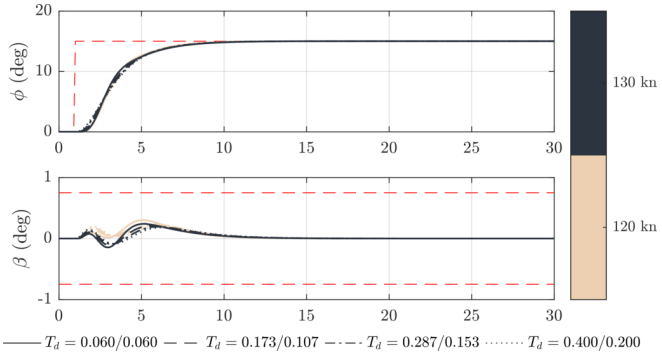

Fig. 12: Roll angle step response in no-fault conditions with K-FTC.

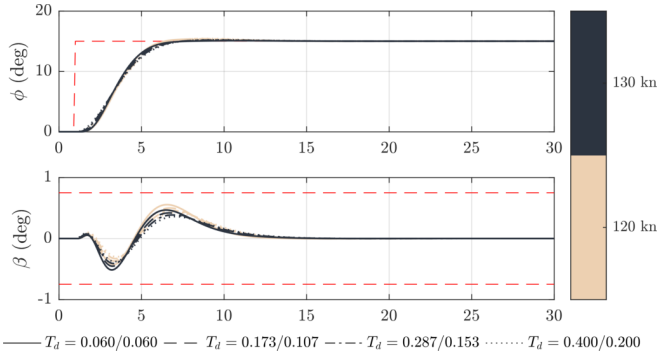

Fig. 13: Roll angle step response with 40% aileron LoE fault with K-FTC.

t = 1000 s. The bank angle response is seen to deteriorate at around 50% LoE, leading to overshoot in the roll angle tracking. The sideslip response also suffers, with increased settling time and decoupling issues.

V. HIL VALIDATION

In this section are presented the results of the HIL tests, and focus is given to the deterioration in performance in the presence of faults. For this assessment, the LoE fault was simulated in software as a simple gain variation for each actuator. The HIL verification activities for MuPAL-α are actually performed with the full aircraft in the hangar, connecting the Fly-By-Wire (FBW) computer directly to a host computer which calculates MuPAL-α's motion under various wind gust conditions (no wind condition, Dryden model wind gust condition, and isolated wind gust condition). Of course, before the HIL tests can be carried out the designed flight controllers must be ported to the correct flight C-code format. This porting includes implementing the designed controllers as discrete-time systems (using a bilinear transform with a sample time of 0.02 seconds). Fig. 15 shows the response of the robust controller K-ROB to doublets in roll angle and sideslip, for different levels of simultaneous aileron and rudder LoE, at an airspeed of 120 knots. It is clear that the responses above 50% fault are inadequate, with too much overshoot in the roll angle channel and a poor settling time and decoupling in the sideslip channel. Fig. 16 shows the results for the same test conditions, but this time with K-FTC instead of the nominal controller. It can be seen that the responses at 50% LoE have improved, with less overshoot in the roll angle and faster rise time in the sideslip channel. The response at 80% LoE still presents a significant overshoot in the roll angle and is too slow in the sideslip channel.

VI. CONCLUSION

This article has presented the design of a robust and a fault-tolerant Y* controller for the lateral/directional motion of the MuPAL-α aircraft. The controllers are designed to be robust against actuator time delays, flight condition variations (i.e. airspeed) and, in the case of the latter, also against loss-of-efficiency faults. The resulting controllers are verified through frequency- and time-domain analysis with linear models, and then validated using MuPAL-α's hardware-in-the-loop capabilities. The comparison between both controllers indicates that K-FTC is able to outperform K-ROB in faulty scenarios, which was expected. The results reinforce the advantage of taking fault scenarios into account from the design phase, as well as the ability of the H_∞ framework to tackle such specifications.

This work has considered the case of efficiency faults on both aileron and rudder actuators. Nonetheless, the strategy could also be applied to deal with additional fault scenarios in multiple actuators without excessive increase in complexity, as the faults/actuators are not independently treated. On the

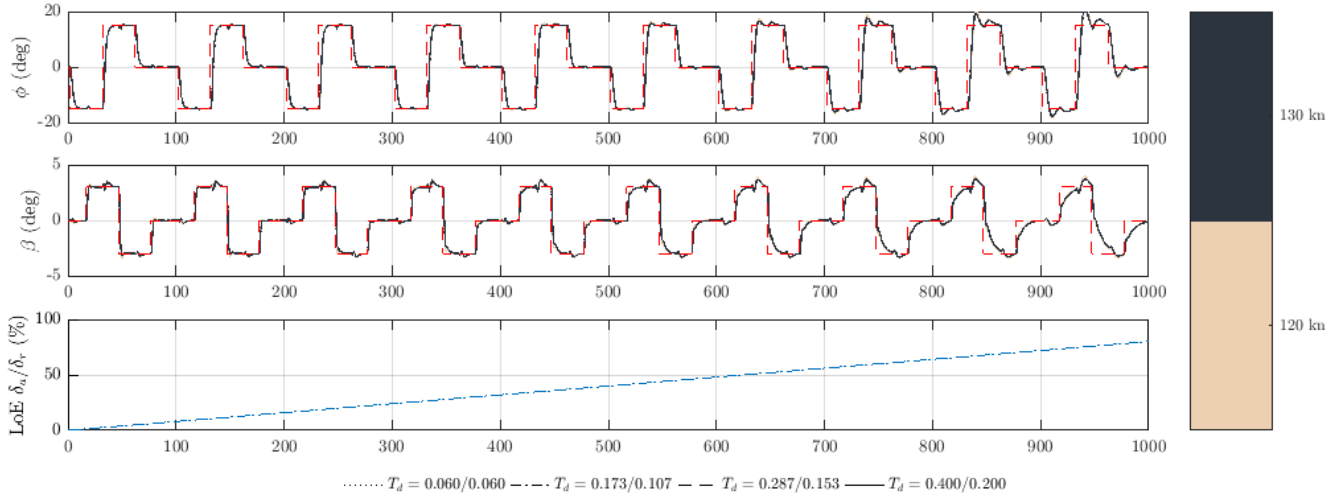

Fig. 14: Doublet maneuvers with increasing aileron and rudder LoE for K-FTC.

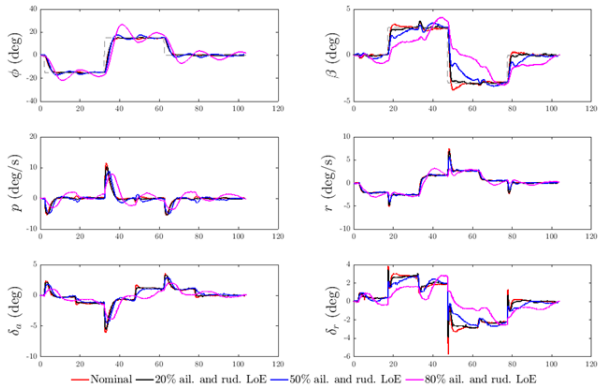

Fig. 15: HIL results with K-ROB and increasing simultaneous aileron and rudder LoE.

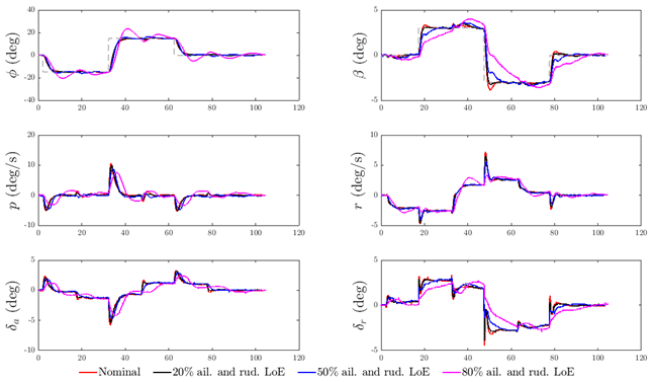

Fig. 16: HIL results with K-FTC and increasing simultaneous aileron and rudder LoE.

downside, such cases could lead to conservatism, since the controller needs to perform consistently in a wide array of scenarios. Some additional trade-off between performance and fault tolerance is then to be expected.

Future work within the framework of the VISION project will be directed towards the extension of the fault-tolerance capabilities by considering switching/scheduling of controllers with respect to some measured fault signals.

References

[1] M. Sato and A. Satoh, "Flight control experiment of Multipurpose-Aviation-Laboratory-α in-flight simulator," *Journal of Guidance, Control, and Dynamics*, vol. 34, no. 4, pp. 1081–1096, 2011.

[2] P. Apkarian, D. Noll, and A. Rondepierre, "Mixed H_2/H_∞ control via nonsmooth optimization," *SIAM Journal on Control and Optimization*, vol. 47, no. 3, pp. 1516–1546, 2008.

[3] C. Favre, "Fly-by-wire for commercial aircraft: the Airbus experience," *International Journal of Control*, vol. 59, no. 1, pp. 139–157, 1994.

[4] E. Field, "The application of a C* flight control law to large civil transport aircraft," College of Aeronautics, Cranfield Institute of Technology, Report 9303, 1993.

[5] P. Gahinet and P. Apkarian, "Structured H_∞ synthesis in MATLAB," *IFAC Proceedings Volumes*, vol. 44, no. 1, pp. 1435–1440, 2011, 18th IFAC World Congress.

[6] P. Apkarian and D. Noll, "Nonsmooth H_∞ synthesis," *IEEE Transactions on Automatic Control*, vol. 51, no. 1, pp. 71–86, Jan 2006.

[7] M. Gabarrou, D. Alazard, and D. Noll, "Structured flight control law design using non-smooth optimization," in *IFAC Symposium on Automatic Control in Aerospace*, vol. 43, no. 15, 2010, pp. 536–541.

[8] H. Lhachemi, D. Saussié, and G. Zhu, "A structured H_∞-based optimization approach for integrated plant and self-scheduled flight control system design," *Aerospace Science and Technology*, vol. 45, pp. 30–38, 2015.

[9] G. Puyou and P. Ezerzere, "Tolerance of aircraft longitudinal control to the loss of scheduling information : toward a performance oriented approach," in *IFAC Symposium on Robust Control Design*, vol. 45, no. 13, 2012, pp. 393–399.

[10] G. Puyou and J.-M. Biannic, "Application of robust antiwindup design to the longitudinal aircraft control to cover actuator loss," *IFAC Proceedings Volumes*, vol. 46, no. 19, pp. 506–511, 2013, 19th IFAC Symposium on Automatic Control in Aerospace.

[11] J. Ackermann, *Uncertainty and Control*, ser. Lecture Notes in Control and Information Sciences. Berlin Heidelberg: Springer-Verlag, 1985, vol. 70, ch. Chapter 4: Multi-Model Approaches to Robust Control System Design, pp. 108–130.